

A Force Balance Model for the Size Prediction of Droplets Formed at T-junction with Xanthan Gum Solutions

Z.P. Gu and J.L. Liow

School of Engineering and Information Technology
University of New South Wales, Canberra@ADFA, Canberra, ACT 2600

Abstract

Microfluidic droplet formation at a T-junction in the jetting regime was studied theoretically and an analytical force balance model was proposed to predict the diameter of droplets. The forces governing droplet production in the jetting regime include the shear, interfacial tension, linear momentum and inertial forces. Experiments were carried with non-Newtonian xanthan gum solutions as the dispersed phase. The model predicted the diameters for both the experimental results and published results in the literature to within $\pm 20\%$. This result is reasonable considering that no fitting parameters were used, and the reasons for this error are discussed. The magnitudes of the forces controlling droplet formation process are also compared in the paper.

Introduction

Microfluidic devices are a promising tool for the production of droplets with a narrow size range. Currently, a number of microfluidic methods have been developed for this purpose, and they include T-junctions [1], flow-focusing devices [2], co-flow devices [3] and microchannels with terraces [4]. The T-junction is the most frequently employed and extensively studied microfluidic geometry and it produces mono-dispersed droplets that are regularly spaced in the outlet stream by shearing a fluid exiting a side stream with a cross-flow of another fluid in the main channel, both of which are immiscible with each other.

Microdroplets generated with a predictable and controllable diameter and size variation have uses in drug delivery and chemical analysis. The parameters found to control the droplet size and size variation include the geometry and dimensions of the microfluidic devices, properties of liquids, flow rates of the two immiscible fluids and surfactant concentration. Numerous investigations have been carried out to examine the effect of these controlling parameters for varying values of the Capillary number ($Ca = u_c \mu_c / \sigma$, where u_c is the velocity of the continuous phase, μ_c the viscosity of the continuous phase and σ the interfacial tension); the dominant dimensionless parameter.

The formation of droplets in a microchannel has been classified as moving from squeezing, through dripping to jetting as the Ca number increases. The squeezing regime results in plug formation at the T-junctions (typically with a $Ca < 0.01$) where the dynamics is controlled by a balance between the interfacial tension and pressure drop across the emerging plugs. The dynamics for the dripping regime ($0.02 < Ca < 0.2$) is governed by the balance between the shear stress and interfacial tension. The jetting regime dominates for $Ca > 0.3$, where the droplet formation is controlled by a shear-driven mechanism.

Currently, most of the studies have concentrated on droplet formation in the squeezing regime with a lack of information in the jetting regime. Droplets generated in the jetting regime are normally accompanied by a long filament joining the forming droplet to the dispersed phase source. This filament is unstable and eventually results in the formation of secondary droplets

leading to a bimodal droplet size distribution. The use of high continuous to dispersed flow rate ratios in the jetting regime leads to a reduction in droplet diameter and a corresponding increase in the droplet formation frequency.

Non-Newtonian fluids have been ignored by previous researchers in microdroplet formation as their high viscosities, elastic behaviour and large molecular weights severely complicate the analysis. However, considering the extensive application of non-Newtonian fluids in the biological and pharmaceutical areas, it is of importance to study non-Newtonian droplet generation. Xanthan gum is a typical shear thinning fluid with properties similar to blood plasma. Gu and Liow [10] have used xanthan gum solutions as the dispersed phase to produce microdroplets.

Hitherto, the lack of understanding of the controlling mechanism makes predicting the droplet size difficult. In this paper, the forces governing droplet formation in the jetting regime were analysed. An analytical force balance model was developed to predict droplet diameter to compare with the experimental results of Gu and Liow [10]. The shear thinning property was also included by the model. Finally, the model was compared with measured experimental data as well as published data of other researchers [12, 13].

Forces analysis for droplets generated in the jetting regime

Droplets formed in the jetting regime (as shown in figure 1) experience the shear, interfacial tension, linear momentum and inertial forces. In this model, the growing droplet is assumed to remain spherical during the entire droplet formation process.

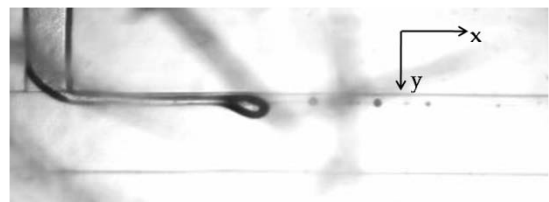


Figure 1. Droplets generated in the microchannel governed by the jetting regime.

Shear Force

The growing droplet is subjected to the hydrodynamic shear force imposed by the continuous phase flow in the main channel. As the flow is laminar ($Re < 0.5$) in the rectangular channel, a parabolic flow profile solution is assumed [5-7]. The local liquid velocity at the centre of the droplet can be approximated as

$$u^* = 2u \left[1 - \left(\frac{D_m - D_D}{D_m} \right)^2 \right], \quad (1)$$

where u is average velocity in the continuous phase channel (m/s) after the T-junction taking into consideration the total flow of both the continuous and dispersed phases, D_D is the diameter of

the droplet (m) and D_m is the hydraulic diameter of the main channel (m).

In the jetting regime, the dispersed phase flow rate is significantly smaller than that of the continuous phase flow rate. Hence the flow in the main channel can be approximated as u_c (the continuous phase velocity, m/s) to give

$$u^* = 2u_c \left[1 - \left(\frac{D_m - D_D}{D_m} \right)^2 \right]. \quad (2)$$

In the jetting regime, the relatively small size of the droplet compared to the microchannel means that the droplet does not obstruct the flow of the continuous phase and hence the pressure drop across the droplet is minimal. The shear force, acting in the positive x -direction is given by

$$F_S = \frac{1}{2} C_D \rho_c (u^* - u_D)^2 A_{eff}, \quad (3)$$

where C_D is the drag force coefficient ($C_D = \frac{24}{Re_D}$ for $Re_D < 1$), ρ_c the density of the continuous phase fluid (kg/m^3), u_D the droplet velocity (m/s) and A_{eff} is the effective cross-sectional area of a droplet as seen by the cross-flow (m^2). Since the droplet is assumed to be spherical, A_{eff} is

$$A_{eff} = \pi \left(\frac{D_D}{2} \right)^2. \quad (4)$$

The modified Reynolds number (Re_D) for the liquid flowing around the drop is given by:

$$Re_D = \frac{\rho_c (u^* - u_D) D_D}{\mu_c}, \quad (5)$$

where μ_c is the continuous phase viscosity (Pa·s).

Experimental observations have shown that the droplet size is dependent on the viscosity of both phases. Based on the Hadamard-Rybczynski solution to a viscous drop in a fluid of different viscosity [8], a viscosity ratio between the dispersed phase and continuous phase ($\lambda = \mu_d / \mu_c$, μ_d is the viscosity of the dispersed phase, Pa·s) is used to modify the drag coefficient giving C_{Def} as:

$$C_{Def} = \frac{8}{Re_D} \frac{3 + 2\lambda}{1 + \lambda}. \quad (6)$$

Substituting equations (2) and (4) into (6) and then (3) gives:

$$F_S = \left(\frac{3 + 2\lambda}{1 + \lambda} \right) \mu_c \left[2u_c \left(1 - \left(\frac{D_m - D_D}{D_m} \right)^2 \right) - u_D \right] (\pi D_D). \quad (7)$$

The droplet velocity (u_D) is not known and is usually taken as a factor (ψ) of u_c and ψ varies from 0 to 2 [5, 9]

$$u_D = \psi u_c. \quad (8)$$

ψ was set to be 0.6 by Husny and Cooper-White [5] as they claimed that this value was representative of the actual drop velocities recorded at times approaching necking and break-up. They also reported a maximum error of 25% for their predicted drop diameters, which may be caused by setting this parameter constant. Sang *et al.* [9] compared this factor against simulation and analytical results for different fluids systems including Newtonian/Newtonian, Newtonian/power law and Newtonian/Bingham. They suggested that ψ was dependent on the viscosity ratio and D_D/D_m and a small change in ψ (5%) brought about a 20% error in predicting the droplet diameter. The scarcity of studies on the droplet velocity currently leaves a gap in the

understanding of how best to represent ψ . Studies that correlated u_D to u_c resulted in a constant predicted drop diameter and is unable to capture the effect of a varying dispersed phase flow rate. In contrast, Qiu *et al.* [14] correlated the droplet velocity to the dispersed phase velocity by a factor of $(D_i/D_f)^2$, where D_i (m) is the hydraulic diameter of the dispersed phase inlet channel, and D_f (m) is the diameter of the filament. The predicted drop diameter was satisfactory even for experiments with a significantly high continuous phase velocity.

During droplet formation, the droplet is linked to the source by a filament which is of comparable diameter to the dispersed phase flow channel dimension. Since the continuous phase flow is assumed to be parabolic and droplets always flow close to the boundary, the droplet velocity is less influenced by the continuous phase flow. Therefore, it is reasonable to correlate the droplet velocity to the dispersed phase velocity as below

$$u_D = \zeta u_d. \quad (9)$$

with ζ to be fixed.

In this paper, the average droplet velocity was measured from the drop formation pictures at 3000 frames/second. Our results show that ζ generally varies from 1 to 3 which do show that the droplet velocity is accelerated by the continuous phase flow. Nevertheless, measurements also suggest that ζ is close to unity for the more viscous xanthan gum solutions. Therefore, ζ is set to be 1 in this paper.

Substituting equation (9) into (7) gives

$$F_S = \left(\frac{3 + 2\lambda}{1 + \lambda} \right) \mu_c \left[2u_c \left(1 - \left(\frac{D_m - D_D}{D_m} \right)^2 \right) - u_d \right] (\pi D_D) \quad (10)$$

Interfacial tension

The interfacial tension (F_σ) acts in the negative x -direction. Given that the filament attached to the growing drop is of similar dimensions to the dispersed phase inlet channel, the interfacial tension force is

$$F_\sigma = \pi \sigma D_i, \quad (11)$$

where σ is the interfacial tension (N/m).

Linear momentum

The linear momentum force (F_L) is caused by the flow momentum of the dispersed phase. Although the linear momentum force is normally neglected by models used for predicting bubble formation, the larger density of the liquid dispersed phase will have a non-negligible contribution. Linear momentum acts in the positive x -direction

$$F_L = \frac{\pi}{4} \rho_d u_d^2 D_i^2, \quad (12)$$

where ρ_d is the density of the dispersed phase (kg/m^3).

Inertia

The liquid inertia force (F_I) is associated with the acceleration of liquid caused by the droplet motion and expansion. Similar to previous works [5, 6], the relative velocity of the continuous phase and dispersed phase during droplet formation is used in the formulation of the liquid inertia force and is given by

$$\begin{aligned} F_I &= \rho_c Q_d (u_D - u^*) \\ &= \rho_c Q_d \left[u_d - 2u_c \left(1 - \left(\frac{D_m - D_D}{D_m} \right)^2 \right) \right], \end{aligned} \quad (13)$$

where Q_d (ml/hr) is the dispersed phase flow rate. In the jetting regime, the droplet velocity is smaller than the continuous phase velocity, hence $(u_D - u^*)$ is usually negative. Therefore, the inertia force attaches the droplet to the dispersed phase and acts in the negative x -direction.

The droplet size at detachment is then controlled by a balance of the respective forces as shown below

$$F_\sigma = F_S + F_L + F_I \quad (14)$$

The sensitivity to ζ was found to be small where the predicted drop size difference was 5.0% for water and 2.0% for 0.5 wt% xanthan gum solution when ζ was varied from 1 to 3. Therefore, the assumption that the droplet velocity equals to the dispersed phase velocity is a reasonable assumption.

Shear thinning properties

Xanthan gum solution is a typical shear thinning fluid and its viscosity varies with shear rate. The rheological behaviour can be correlated using the power law equation below

$$\mu = k\dot{\gamma}^{n-1}, \quad (15)$$

where μ is the viscosity (Pas), k the consistency index ($\text{Pa}\cdot\text{s}^{n-1}$), $\dot{\gamma}$ the shear rate (s^{-1}), and n the power-law index.

The continuous phase velocity is assumed to be constant here, and the shear rate can be calculated as follow:

$$\dot{\gamma} = \frac{u_c}{w_m}. \quad (16)$$

where w_m is the width of the main channel (m).

Substituting equation (15) into (16) gives the dispersed phase viscosity as

$$\mu_d = k \left(\frac{u_c}{w_m} \right)^{n-1}. \quad (17)$$

Result and discussion

The theoretical model was validated by comparing it with the experimental data of Gu and Liow [10] and details of the experimental procedures can be found there. Figure 2 compares the experimental diameter with the predicted diameter for a variety of dispersed phases used, including water and xanthan gum solutions with concentrations from 0.01 to 0.5 wt%.

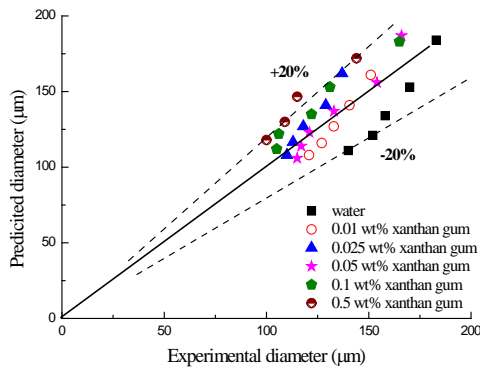


Figure 2. Comparison between the predicted and experimental diameters for a variety of dispersed phases. The solid line represents an exact prediction with $\pm 20.0\%$ error represented by the dashed lines.

The predicted droplet diameters lie within $\pm 20.0\%$ of the measured values. This result is reasonable as the accuracy of the experimental data is sensitive to the accuracy of the method for measuring the droplet diameters, which can be difficult when the

droplets are very small. The errors can partly be attributed to the difficulty in estimating droplet diameters from images where the pixel resolution is limited. Another factor is that the viscosities of the xanthan gums are dependent on the shear rate. The model assumes an average shear rate and hence does not fully take into account the possibility of high shear rates nearer the boundary.

A common procedure in microfluidic experiments is to use silicone tubing to connect a syringe, operated by a syringe pump, to a metal tubing linked to the microfluidic device. The silicone tubing can swell and deliver a flow rate different from the set value at the syringe pump. This problem is exacerbated when a high pressure is required to achieve a large flow rate. van der Graaf *et al.* [11] confirmed that the applied flow rate is not always the same as the flow rate calculated from the sizes and numbers of formed droplets, especially at high flow rates. The continuous phase flow rates employed by Gu and Liow [10] were very high and were not corrected which can lead to the errors in the comparison.

Additionally, it is known that the interfacial tension exhibits a dynamic behaviour and it takes around 1 second before the equilibrium value is reached. However, the formation time for droplets governed by the jetting regime can be as short as 50 ms, which is shorter than the time needed before the interfacial tension gets equilibrated. However, as there is insufficient understanding of the dynamic behaviour of droplet generation, most studies still treat the interfacial tension as constant throughout the formation process. Nevertheless, the results suggest that the model developed can successfully predict the droplet size formed at a T-junction generator in the jetting regime without the need to employ any fitting parameters to the force balance.

Comparison of the model with published data

The model was also tested on other published data [5, 12, 13], ranging from experiments to computer simulations performed in the jetting regime. These data covers a wide range of conditions including various T-junction dimensions, different physical properties of both phases, and operating parameters such as flow rate.

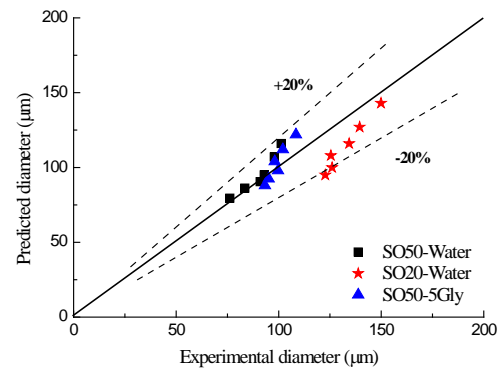


Figure 3. Comparison between the predicted and experimental diameters from Husny and Cooper-White [5]. The solid line represents an exact prediction with $\pm 20.0\%$ error represented by the dashed lines. “SO” is silicone oil. “5 Gly” is a 5 wt% glycerol in water.

Figures 3 and 4 present the prediction for external data set from Husny and Cooper-White [5], Liow [12] and Yeom and Lee [13]. As the data from Husny and Cooper-White [5] covers a range of continuous phases and dispersed phase liquids, it is plotted separately in figure 3. Generally, the predictions are satisfied as most of the data fall within an error range of $\pm 20.0\%$, which is

quite good considering no fitting parameters were employed in this model. The results demonstrate the model presented in this paper can successfully predict not only our experiments, but also other published data, such as has not been achieved by previous models.

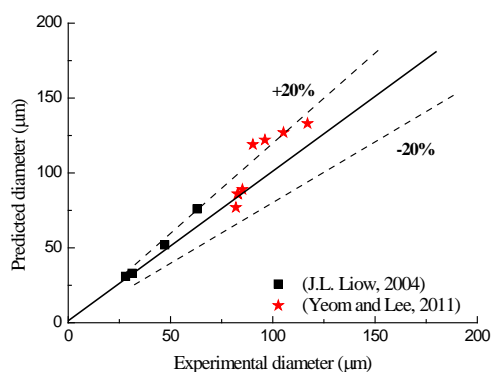


Figure 4. Comparison between the predicted and experimental diameter from references [12] and [13]. The solid line represents an exact prediction with $\pm 20.0\%$ error represented by the dashed lines.

Comparison of the magnitude of the controlling forces

The magnitudes of the individual forces acting on the droplet are shown in figure 5 for a flow rate ratio (Q_c/Q_d) of 100.

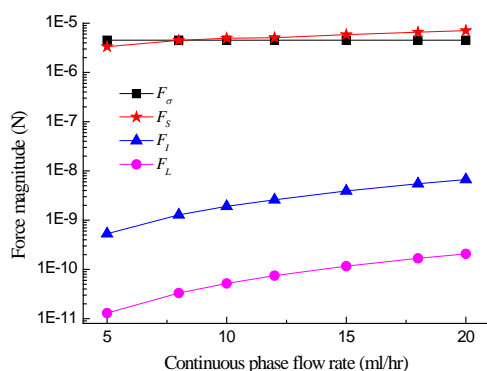


Figure 5. Comparison of the magnitude of controlling forces, where F_σ is the interfacial tension force, F_S is the shear force, F_I is the inertia force and F_L is the linear momentum force.

Figure 5 shows that droplet generation is mainly governed by the interfacial tension and shear forces, whose magnitudes are of similar order. The interfacial tension force is independent of Q_c , while as the continuous phase flow rate increases from 5.0 to 20.0 ml/hr, there is a doubling in the shear force. Although the dimension of the inertial force is at least three orders smaller than that of the interfacial tension and shear force, it has a small effect on droplet production especially at high continuous phase flow rates. The effect of the linear momentum can be neglected, being five to six magnitudes smaller.

Conclusions

Microfluidic droplet formation has been researched extensively due to their far-reaching applications. However, there is a scarcity of models on predicting the diameter of droplet produced in the microchannel.

In this study, microfluidic droplet formation at a T-junction in the jetting regime was studied theoretically and an analytical force balance model was proposed to predict the diameter of droplet. The forces governing droplets generation in the jetting regime include the shear, interfacial tension, linear momentum and inertial forces. Experiments with non-Newtonian xanthan gum

solutions as the dispersed phase were used to test the developed model. The model was able to predict the diameters for author's experimental results as well as published results to within $\pm 20.0\%$. This result is reasonable and the sources for the discrepancy were discussed. The magnitudes of the forces controlling the droplet formation process were also compared.

Acknowledgements

Z.P. Gu gratefully acknowledges the financial support from the Chinese Scholarship Council.

References

- [1] Glawdel, T., Elbuken, C. and Ren, C.L., *Droplet formation in microfluidic T-junction generators operating in the transitional regime. I. Experimental observations*. Physical Review E, 2012. 85(1): p. 016322 (1–9).
- [2] Fu, T.T., et al., *Scaling the formation of slug bubbles in microfluidic flow-focusing devices*. Microfluidics and Nanofluidics, 2010. 8(4): p. 467–475.
- [3] Cramer, C., Fischer, P. and Windhab, E.J., *Drop formation in a co-flowing ambient fluid*. Chemical Engineering Science, 2004. 59(15): p. 3045–3058.
- [4] Sugiura, S., et al., *Novel method for obtaining homogeneous giant vesicles from a monodisperse water-in-oil emulsion prepared with a microfluidic device*. Langmuir, 2008. 24(9): p. 4581–4588.
- [5] Husny, J. and Cooper-White, J.J., *The effect of elasticity on drop creation in T-shaped microchannels*. Journal of Non-Newtonian Fluid Mechanics, 2006. 137(1–3): p. 121–136.
- [6] Nahra, H.K. and Kamotani, Y., *Bubble formation from wall orifice in liquid cross-flow under low gravity*. Chemical Engineering Science, 2000. 55(20): p. 4653–4665.
- [7] Qiu, D.M., et al., *Micro-droplet formation in non-Newtonian fluid in a microchannel*. Microfluidics and Nanofluidics, 2010. 8(4): p. 531–548.
- [8] Rybczynski, W., *Translatory motion of a fluid sphere in a viscous medium*. Bull. Int. Acad. Pol. Sci. Leu., CI Sci. Nat. Ser. A, 1911. p. 40–46.
- [9] Sang, L., Hong, Y.P., and Wang, F.J., *Investigation of viscosity effect on droplet formation in T-shaped microchannels by numerical and analytical methods*. Microfluidics and Nanofluidics, 2009. 6(5): p. 621–635.
- [10] Gu, Z.P. and Liow, J.L., *Microdroplet formation in a T-junction with xanthan gum solutions*. CHEMECA 2011, 18–21 September 2011, Sydney, NSW, Australia.
- [11] van der Graaf, S., et al., *Droplet formation in a T-shaped microchannel junction: A model system for membrane emulsification*. Colloids and Surfaces a-Physicochemical and Engineering Aspects, 2005. 266(1–3): p. 106–116.
- [12] Liow, J.L., *Numerical simulation of drop formation in a T-shaped microchannel*. Paper AFMC 00019. 15th Australasian Fluid Mechanics Conference, 13–17 December 2004, Sydney, NSW, Australia.
- [13] Yeom, S. and Lee, S.Y., *Size prediction of drops formed by dripping at a micro T-junction in liquid-liquid mixing*. Experimental Thermal and Fluid Science, 2011. 35(2): p. 387–394.
- [14] Qiu, D., Silva, L., Tonkovich, A. L. and Arora, R. *Micro-droplet formation in non-Newtonian fluid in a microchannel*. Microfluidics and Nanofluidics, 2010. 8: p.531-548.